



Full length article

A comparative study of bio-inspired protective scales using 3D printing and mechanical testing



Roberto Martini, Yanis Balit, Francois Barthelat*

Department of Mechanical Engineering, McGill University, 817 Sherbrooke Street West, Montreal, QC H3A 2K6, Canada

ARTICLE INFO

Article history:

Received 13 December 2016
 Received in revised form 15 February 2017
 Accepted 14 March 2017
 Available online 16 March 2017

Keywords:

Fish scales
 Osteoderms
 Bioinspiration
 Dermal armor
 3D printing

ABSTRACT

Flexible natural armors from fish, alligators or armadillo are attracting an increasing amount of attention for their unique combinations of hardness, flexibility and light weight. The extreme contrast of stiffness between hard scales and surrounding soft tissues gives rise to unusual and attractive mechanisms, which now serve as models for the design of bio-inspired armors. Despite this growing interest, there is little guideline for the choice of materials, optimum thickness, size, shape and arrangement for the protective scales. In this work, we explore how the geometry and arrangement of hard scales can be tailored to promote scale-scale interactions. We use 3D printing to fabricate arrays of scales with increasingly complex geometries and arrangements, from simple squares with no overlap to complex ganoid-scales with overlaps and interlocking features. We performed puncture tests and flexural tests on each of the 3D printed materials, and we report the puncture resistance – compliance characteristics of each design on an Ashby chart. The interactions between the scales can significantly increase the resistance to puncture, and these interactions can be maximized by tuning the geometry and arrangement of the scales. Interestingly, the designs that offer the best combinations of puncture resistance and flexural compliance are similar to the geometry and arrangement of natural teleost and ganoid scales, which suggests that natural evolution has shaped these systems to maximize flexible protection. This study yields new insights into the mechanisms of natural dermal armor, and also suggests new designs for personal protective systems.

Statement of Significance

Flexible natural armors from fishes, alligators or armadillos are attracting an increasing amount of attention for their unique and attractive combinations of hardness, flexibility and low weight. Despite a growing interest in bio-inspired flexible protection, there is still little guideline for the choice of materials, optimum thickness, size, shape and arrangement of the protective scales. In this work, we explore how the geometry and arrangement of hard scales affect puncture resistance and flexural compliance, using 3D printing and mechanical testing. Our main finding is that the performance of the scaled skin in terms of puncture resistance can be significantly improved by slight changes in their geometry and arrangement. Our results also suggest that natural evolution has shaped scaled skins to maximize flexible protection. This study yields new insights into the mechanics of natural dermal armors, and also suggests new designs for personal protective systems.

© 2017 Acta Materialia Inc. Published by Elsevier Ltd. All rights reserved.

1. Introduction

Materials for personal protection against laceration or puncture must be hard to prevent penetration, yet soft to allow for flexural deformations and unimpeded movement. These conflicting requirements in materials selection have been resolved in nature millions of years ago with the emergence of dermal armors made

of stiff plates of finite size embedded in soft, flexible tissues. All groups in the animal kingdom include species with highly evolved protective systems against predators, territorial challengers, collisions or other mechanical threats [1]. External protective systems range from thin, flexible but tough proteinaceous skins in mammals [2] to thick, highly mineralized and hard shells in molluscs [3]. The intermediate solution, which is also found in a large variety of animal species, consist of articulated hard protective elements of finite size [4]. These segmented armor systems provide high surface hardness to prevent puncture, yet they provide some

* Corresponding author.

E-mail address: francois.barthelat@mcgill.ca (F. Barthelat).

flexibility to allow movements and fast locomotion. Examples of segmented armor include teleost fish scales (Fig. 1a), ganoid scales (Fig. 1b) and bony plates (osteoderms, Fig. 1c). Segmented armors are based on “Universal” construction principles: they consist of rigid plates (or scales) protecting soft substrates (deeper layers of skin, muscles and internal organs) which are 1–5 orders of magnitude softer than the protective plates [5]. A closer examination, however, reveals a large variety of materials, shape, size, arrangement and overlap across animal species, and a rich set of deformation and failure mechanisms associated with plate fracture [6–8] and puncture [9–11], plate stability [12], plate-substrate interactions and plate-plate interactions [13–18]. Each scale can be made of distinct materials with a multilayered arrangement which generates high surface hardness combined with high toughness [14,19]. Recent studies also highlighted the effect of the size of the scales, smaller scales being more difficult to fracture because of their reduced flexural span [5]. Puncture tests on individual plates on soft substrates have also recently revealed a dangerous failure mode where the plate suddenly tilts under the action of the indenter, cancelling its protective function and exposing the substrate [5]. This “tilting” failure mode, also observed in the scaled skin of alligator gar fish, was studied in details using contact mechanics and experiments [12]. The interaction between scales is critical during puncture, because neighboring scales can redistribute stresses in the substrate [5] or generate overlaps and interlocks for a continuous protection [20]. The materials, shape, size and arrangement of the scales also influence the flexural response of the whole scaled skin. For example, scale-scale interactions in fish skins are weak for small flexural deformations, but become stronger at large skin curvatures, generating a stiffening effect in flexion [21,22,15].

Fish scales and osteoderms are now inspiring the development of novel protective systems fabricated using 3D printing of polymers [15,17] or ceramics [23], laser engraving of glass and ceramics, stretch-and-release methods to generate overlaps [24].

Despite these recent efforts and the potential of bio-inspiration in new flexible protective systems, there are still no clear guidelines to design and optimize the shape and arrangement of the scales to simultaneously maximize protection and flexural compliance. In this work, we present the first systematic study of how the shape of the rigid scales affects the flexibility, the puncture resistance and the homogeneity of the puncture resistance of segmented armors. The objective was to explore how the shape and arrangement of hard scales on soft substrates can increase the

puncture resistance of scaled skin, while maintaining high flexural compliance.

2. Overview of mechanics and geometries

Fig. 2a shows a two-dimensional diagram of a hard scale resting on a soft substrate. Although we do not present any measurement of hardness in this work, we use the term “hard” for the scales because they are much harder (and stiffer) than the substrate, so that the deformations of the scales are negligible compared to deformations of the substrate. An indenter exerts a vertical force on the surface of the scale, in the most general case at an offset distance from the center of the scale. In the case of interest where the scale is stiff and the substrate is compliant, the substrate will progressively tilt as the force is increased [12]. To simplify the problem, all forces shown on Fig. 2a are assumed to be vertical (including the reaction forces from the substrate), which implies that the substrate can slide freely along the horizontal direction relatively to the indenter. The vertical point force may be decomposed into a force N normal to the scale, and a friction force T tangent to the scale. To sustain this equilibrium position, the tip of the indenter must not slide on the surface of the scale and, therefore, $T < fN$, [28]. As the tilt angle increases to a critical value $T = fN$ the indenter rapidly slides on the surface of the scale, the scale rapidly tilts and the indenter slips into the soft substrate. This tilting instability is considered a failure mode even if the scale remains undamaged because the sharp indenter has reached the softer substrate. This failure mode was observed experimentally on glass plates [5], ceramic plates [24] and also on the scaled skin of alligator gar fish which are covered with thick and bony ganoid scales [12]. Detailed mechanical models are now available to predict the onset of instability for hard scales on soft substrates [12]. Tilt instability may be delayed by smaller offset distances (a random variable which cannot be controlled in actual applications), stiffer substrates and larger scales (both have negative impacts on flexural compliance), and friction coefficient (which may be increased by tailoring the material and/or morphology of the surface). Here we explore how the interaction between the scales may be another strategy to delay unstable tilting while maintaining flexural compliance. Fig. 2b shows how an indented scale can tilt and jam between the neighboring scales. The contact forces may be asymmetric, and the reaction force from the substrate may have a horizontal component. However, the horizontal components of contact force and substrate reaction must self equilibrate. In this

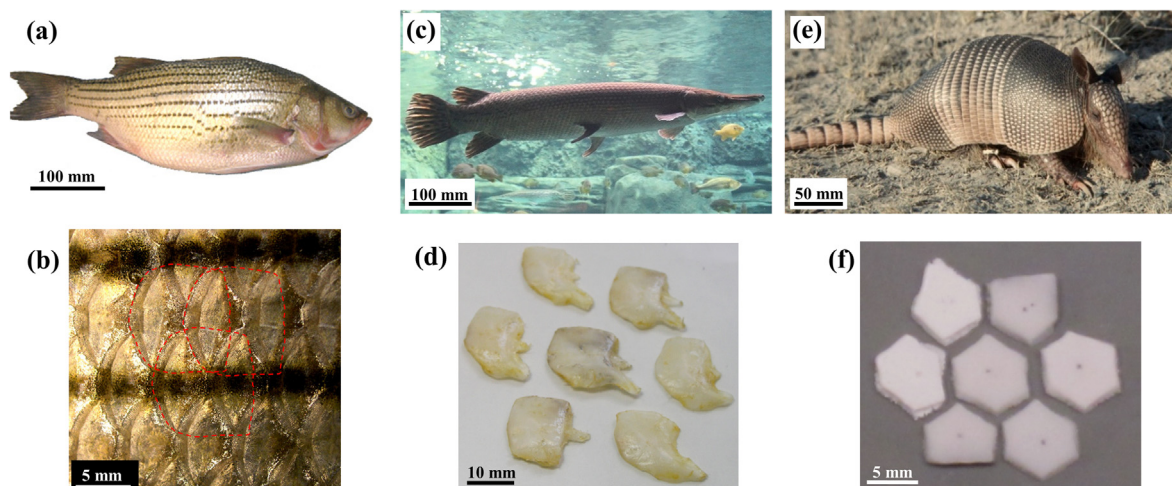


Fig. 1. Examples of segmented armors found in nature: (a),(b) Striped bass with detail of the arrangement of the scales and geometry [25]; (c),(d) Alligator gar with detail of the scales; (e),(f) Armadillo with detail of the bony plates [26,27]

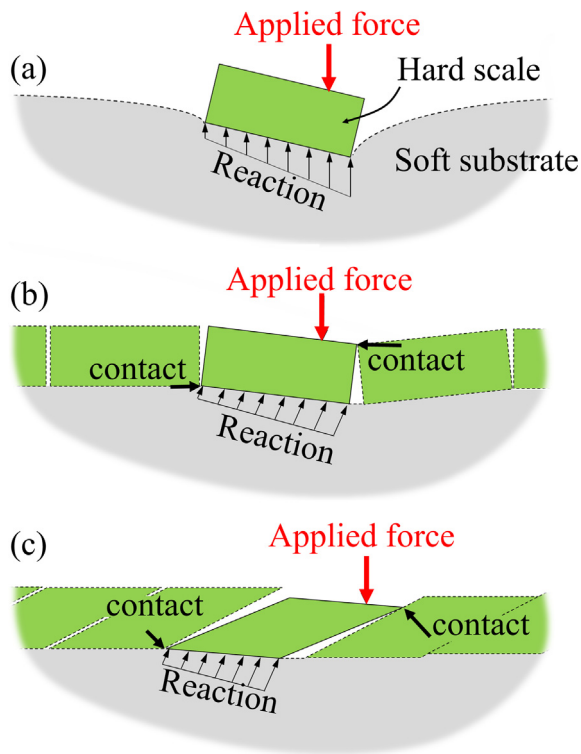


Fig. 2. Two dimensional free body diagrams of scales resting on soft substrates and deflected by a sharp indenter (point force): (a) individual rectangular scale; (b) the same scale, surrounded by identical scales; (c) slanted scales can generate stronger scale-scale interactions, which improves stability.

configuration, the two contact forces are expected to resist tilting and improve stability. Fig. 2c shows scales with a slanted geometry that generate overlaps between neighboring scales. In this configuration the neighboring scale can carry a significant portion of the applied force, through a contact force with a strong vertical component. In turn, the orientation and magnitude of that contact force generates a strong moment on the indented scale which counters the moment generated by the applied force. This geometry would therefore prevent tilting and result in an increase in stability for the indented scale. The purpose of this study is to explore how three dimensional scales of increased complexity in shape and arrangement may stabilize the scales and make the scaled skin more resistant to sharp puncture. The study was based on 3D printing of polymeric models and miniaturized puncture tests. This experimental approach was preferred to computational models, because the large number of scale-scale contacts involved in a puncture event present numerical challenges and convergence difficulties. This approach is also in line with recent work that have used 3D printing to make models and help understand the structure and mechanics of complex natural systems such as the sea-horse tail [4], shark skeletons [29] or teleost scales [15].

Fig. 3 presents an overview of the eight geometries considered in this work. We started from a single, isolated rectangular scale (Fig. 3a), and increased the complexity of the system by adding more scales into arrays, by generating overlap and by enriching the geometry of the scales with bioinspired features: three different overlapping designs (Fig. 3c, d, e), one interlocking design (Fig. 3f) and ganoid-like complex 3D designs (Fig. 3g, h). The most complex geometry considered in this work was 3D printed directly from microCT data from ganoid scales from *polypterus senegalus* [19] (Fig. 3h). In order to isolate the effects of geometry and arrangement, some design parameters were kept constant throughout all the configurations: the set of materials were identi-

cal for all the designs: the scales were made of a relatively stiff polymer (Acrylonitrile butadiene styrene (ABS), modulus $E = 3$ GPa, Poisson's ratio $\nu = 0.35$) which were glued onto a much softer substrate (polyurethane, modulus $E \sim 0.7$ MPa, Poisson's ratio $\nu \sim 0.5$) with a thickness of 3 mm. The thickness of the scales was kept at $t = 2$ mm for all designs, and the surface area of the front face of the scales was kept to a square of size 4 mm by 4 mm for all the designs (except for the topologically interlocked and full ganoid designs where topological constraints forced us to use dimensions close to, but not exactly, 4 mm by 4 mm). The scales were arranged in 5×5 arrays with no gaps between them (except for Fig. 3a where an isolated scale was considered).

3. Fabrication

The fabrication steps for the samples are shown in Fig. 4. Arrays of 5×5 scales with the desired geometry and arrangement (Fig. 3) were 3D printed with an ABS photopolymer and with a high-resolution Direct Light Projector (DLP) 3D printer (Micro HiRes, EnvisionTEC GmbH, Gladbeck, Germany) on sacrificial column-like supports. In order to prevent the scales from fusing together during printing, a gap of 500 μm was left between the scales. After 3D printing, the photo-polymerization of the array of scales was completed with an Otofash (EnvisionTEC) post-curing light pulsing unit, with 6000 flashes/side. This protocol produced fully dense, isotropic ABS scales, with a flexural modulus of about 3 GPa and a flexural strength of about 100 MPa (measured using three-point-bending tests). The array was then compressed transversally using a biaxial vice system to suppress the gap between the scales (step 2). An adhesive tape was applied on the top surface of the scales for tape transfer (step 3) and the scales were released from the sacrificial support using a razor blade (step 4). Finally, the scales were glued on a 3 mm thick polyurethane membrane (modulus $E = 0.7$ MPa measured from three-point bending test) using a cyanoacrylate adhesive (step 5).

Once the adhesive was fully cured, the tape was removed and the surface of the scales was cleaned with ethanol to remove residues from the adhesive tape. The sample was then ready for mechanical tests.

4. Puncture resistance

The puncture tests were performed using the same protocol for all samples. A miniaturized loading stage (Fullam Inc, NY) equipped with a 45 N capacity load cell and mounted with a needle was used for the tests. Preliminary tests used a steel needle, which resulted in plowing and surface damage on the scales [28]. In order to prevent damage and to perform multiple tests on the same sample, we used a needle made of ABS which was 3D printed with the same ABS polymer used for the scales (tip radius = 300 μm). In this conditions, the ABS needle and ABS scales are considered “hard”, because their deformation can be neglected in comparison to the deformations in the substrate. In addition the radius of the indenter and the contact area were small compared to the other dimensions in the system, so that for the purpose of characterizing and predicting the tilting of the indented scales, the contact pressure from the indenter tip was modelled as a point force. For testing, the sample was placed on a 13 mm-thick neoprene substrate (Young's modulus = 0.15 MPa, measured by spherical indentation assuming a Poisson's ratio ~ 0.5), which was itself placed on six steel balls to remove any lateral constraints and cancel lateral forces which would complicate the analysis of the results [12]. Experiments with different substrate thicknesses (not shown here) showed that a 13 mm-thick substrate was beyond the range where substrate thickness affects the indentation results (i.e. we

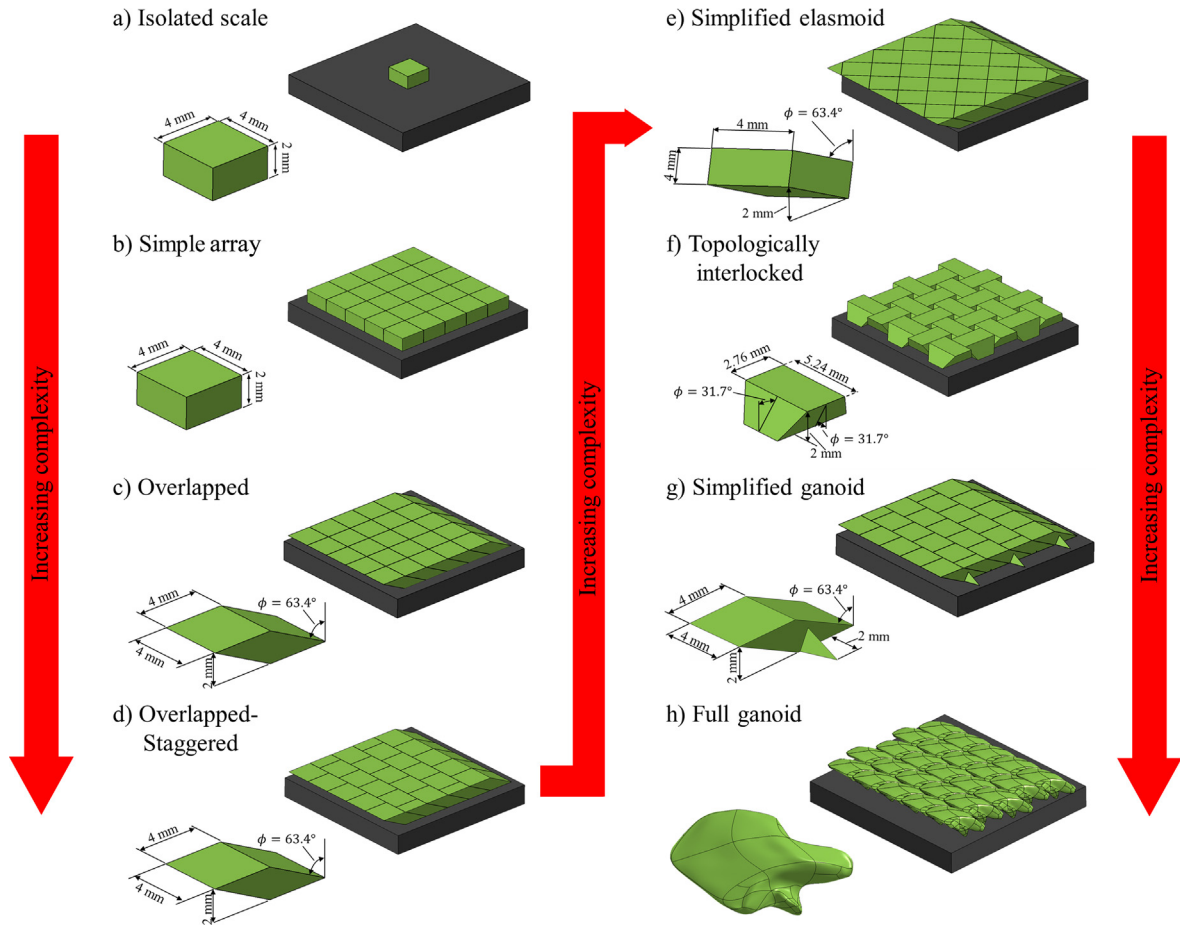


Fig. 3. Schematics of the eight scaled skin designs that were considered in this work, ranked in order of increasing complexity.

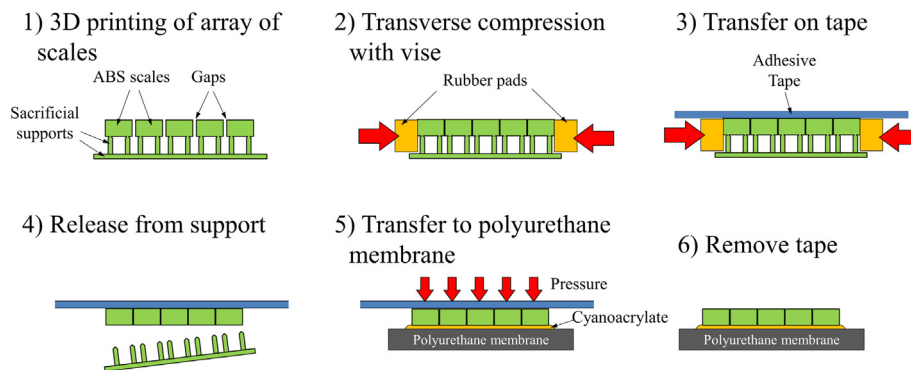


Fig. 4. Fabrication steps for the scaled membrane.

chose the substrate to be thick enough to be considered as a half space). All the tests were performed at a displacement rate of $50 \mu\text{m/s}$. For each design, we punctured the central scale at 30 different locations to take into account the variation of the puncture resistance with offset distance [12]. Pictures were taken during the puncture tests to accurately map the position of the punctures on the scale and to monitor the translations and rotations of the scales during puncture. Fig. 5 shows a set of typical puncture force-displacement curves with their associated mode of failure for an individual scale, and for a 5×5 array of scales (simple array design), with size $2L = 4 \text{ mm}$ and $t = 2 \text{ mm}$. All curves were linear or close to linear up to instability, but the range of results varied

greatly depending on the location of the puncture on the scale. Snapshots of the samples confirmed, for all tests, the mechanisms of scale tilting described above (Fig. 5b). In the simple array design, visual inspection did not reveal any apparent displacement in the eighteen scales located at the periphery of the array. These peripheral scales may undergo small displacement, but these would be negligible compared to the amount of displacement and rotation near the indented site. The puncture force increased linearly with displacement, while we observed the indented scale progressively tilting under the action of the needle (consistent with our previous experiments [12]). At a critical force F_C , the needle suddenly slid on the surface of the scale, which made the scale rapidly tilt until the

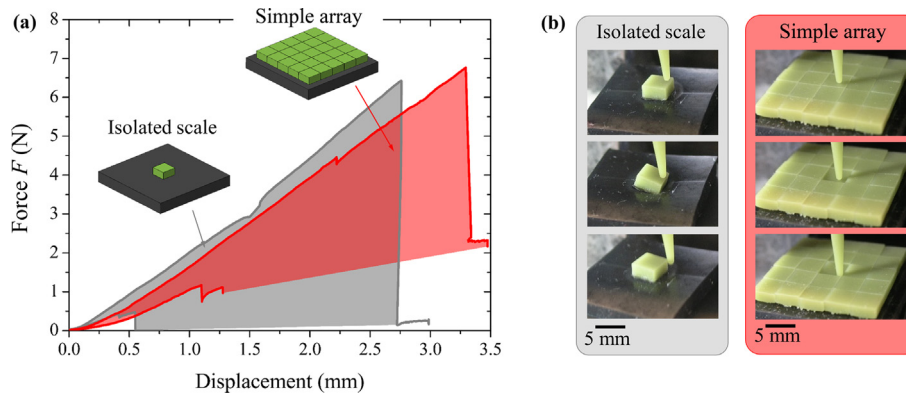


Fig. 5. (a) Range of force displacement curves from puncture experiments on isolated scales and on simple arrays of scales. (b) Corresponding in-situ images showing the deformation of the isolated scale and of the simple array.

needle reached the softer membrane. This unstable event was characterized by a sharp decrease in puncture force. In this event the scaled membrane is considered defeated since the tip of the needle reaches the softer substrate. The maximum force F_c was therefore used as a measure of the puncture resistance of the scaled membrane. The following sections present and discuss the puncture resistance of the designs shown in Fig. 3, in the same order of increasing complexity.

(a) Isolated scales and (b) Simple array of scales: The first question in this study was whether interactions between neighboring scales and the jamming effect illustrated on Fig. 2b could increase puncture resistance. Direct comparison is difficult because of the wide range of puncture responses shown on Fig. 5a. However a large portion of this variation can be explained by puncture location [12], which can be taken into account in the analysis of the results. Fig. 6a shows how a coordinate system (x,y) is attached to the indented scale in order to track the puncture location (δ_x, δ_y) . Fig. 6b and c show maps of the puncture resistance (only one quarter of the scales is showed for symmetry reasons). The puncture resistance is the highest near the center of the scale, and decreases for punctures performed near the edge of the scale. In order to compare the performance of these two designs, the experimental data was fitted with surfaces. The puncture resistance of the isolated scale is proportional to the inverse of the offset distance, in accordance to the semi-analytical model we have recently developed for a circular plate on a soft substrate [12]. More specifically, the puncture force was fitted with:

$$F_c = \frac{\pi f}{1 - \nu^2} \frac{EL^2}{\sqrt{(\delta_x/L)^2 + (\delta_y/L)^2}} \quad (1)$$

where δ_x and δ_y are the positions of the indent in the (x,y) coordinate system (Fig. 6a), E is the Young's modulus of the substrate and L is the size of the scale (Here $E = 0.15$ MPa, $\nu \sim 0.5$ and $L = 2$ mm).

In this work the friction coefficient between the needle and the scale was $f = 0.24$, measured with independent experiments following the method reported in [12]. Even though the scale is square, we verified that the puncture force has no dependence on orientation of the scale, and that the fitting constant match the theoretical prediction [12] well.

In the case of the array of scales, the complex interaction with the neighboring scales causes the behavior to deviate from this simple semi-analytical model. We therefore modified the fitting function to include an angular dependence of the critical puncture force:

$$F_c = 1.34 \frac{\pi f}{1 - \nu^2} \frac{EL^2}{\sqrt{(\delta_x/L)^2 + (\delta_y/L)^2}} (1 + 0.08 \cos(4\theta)) \quad (2)$$

where $\theta = \tan^{-1}(\delta_y/\delta_x)$. The results from fitting Eqs. (1) and (2) are plotted on Fig. 6d, and they can serve as the basis for comparison of the two designs. Both results show how quickly the puncture resistance F_c decreases as the offset distance increases. The interactions with neighboring scales, however, uniformly increase the critical force, with the most pronounced improvements occurring when the offset distance is large. The results from the array of scales also clearly show the angular dependence of the results. In this case a scale indented along the x or the y axis will tilt and interact with only one neighboring scale. The same scale, indented along one its diagonals ($\delta_y = \delta_x$ or $\delta_y = -\delta_x$) will resist tilting better because it interacts with two neighboring scales. An advantage of the fitting surfaces over the experimental results is that an average puncture resistance value can be computed using:

$$\bar{F}_c = \frac{1}{4} \int_{-1}^1 \int_{-1}^1 F_c d(\delta_x/L) d(\delta_y/L) \quad (3)$$

Combining Eq. (3) with Eq. (1) for the isolated scale gives $\bar{F}_c = 0.77$ N. By comparison, combining Eq. (3) with Eq. (2) for the simple array of scales gives $\bar{F}_c = 1.43$ N. Overall, the neighboring scales in the array therefore increase the stability of the scale by about 100 %.

(c) Overlapped and (d) Staggered overlapped designs: In the next part of this study, we enriched the geometry of the individual scales in order to further promote scale-scale interactions, with the objective of further increasing the critical puncture force F_c . A simple approach to generate overlaps between the scales is to slant the side faces of the scales, as shown on Fig. 2c. The design of the scales was the same as in the previous scales ($2L = 4$ mm and $t = 2$ mm), with the addition of slanted side faces at an angle $\phi = 63.4^\circ$ (Fig. 7a). This angle was chosen so that the longest dimension of the scale was $4L = 8$ mm, resulting in a 50% overlap of the scales in the array. We considered two arrangements: a square arrangement identical to the 5×5 array described above (Fig. 3c), and a staggered arrangement where every other row of scale was shifted by L along the y direction (Fig. 3d). The array of scales was then tested for puncture resistance as described above. The shape of the puncture force-deflection curve was the same as before, and a puncture resistance F_c could be measured for each experiment. Fig. 7b and c show the puncture resistance maps for the overlapped scales (Fig. 7b) and the overlapped-staggered scales (Fig. 7c). The overlap has two distinct effects: (i) the region where the scale is

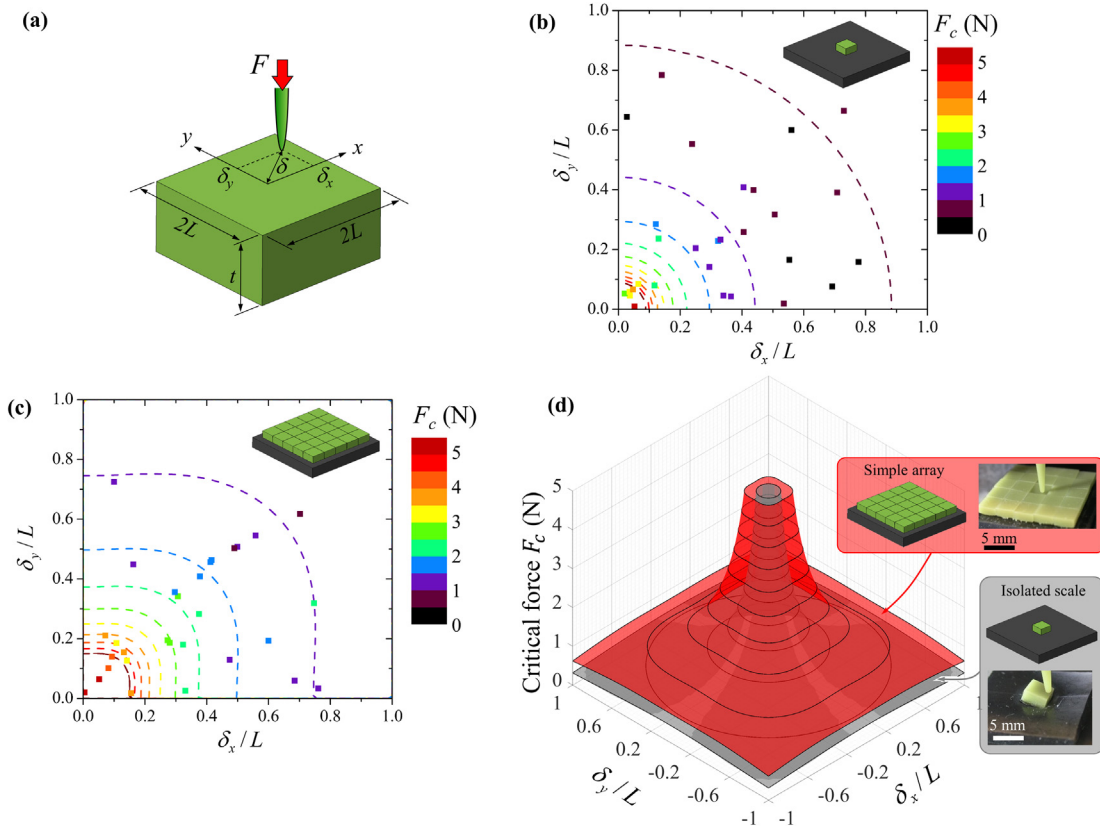


Fig. 6. (a) Diagram of an individual square scale showing dimensions and puncture location at offset coordinates (δ_x, δ_y) ; (b) Experimental critical puncture force F_c as function of location for an isolated scale, and (c) for a 5×5 array of scales; (d) continuous surfaces fitted to the data points shown in (b,c) for easier comparison of the puncture performance of isolated scale and simple array of scale. The 2-norm of the fitting errors for the isolated scale and the array of scales are 3.41 and 2.63, respectively.

the most stable was shifted from $(\delta_x = 0, \delta_y = 0)$ in the previous case to about $(\delta_x = 0.5L, \delta_y = 0)$ in the overlapped design, and to $(\delta_x = L, \delta_y = 0)$ in the overlapped-staggered design. This effect can be explained by the shifting of the base of the scale towards the positive x direction; (ii) The overlap delays tilting but mostly about the y axis, which created a strong orientation effect with tilting occurring preferentially about the x axis. As a result, the contour lines become almost horizontal as δ_y is increased, in contrast with the case shown on Fig. 6b, where the contour lines were concentric circles. For comparison of the designs, experimental data on the overlapped scale array were fitted with:

$$F_c = 6.17 \frac{\pi f}{1 - \nu^2} \frac{EL^2}{\left(0.026 \left(\frac{\delta_x - \delta_{x0}}{L}\right)^2 + \left(\frac{\delta_y}{L}\right)^2\right)^{0.3}} \quad (4)$$

The experimental data on the overlapped-staggered array were fitted with:

$$F_c = 8.17 \frac{\pi f}{1 - \nu^2} \frac{EL^2}{\left(0.004 \left(\frac{\delta_x - \delta_{x0}}{L}\right)^2 + \left(\frac{\delta_y}{L}\right)^2\right)^{0.3}} \quad (5)$$

Fig. 7d shown a comparison of the regular array and staggered designs. The puncture force F_c increases in the $\delta_x/L = -1$ region because the overlap increases the interaction with the neighboring scale (following the mechanism shown on Fig. 2c. F_c also increases in the $\delta_x/L = +1$ region, because the slanted geometry of the scale shifts the base of the scale towards the positive x axis, making it more difficult to tilt toward that direction. This second effect is more pronounced than the first, so that the region of maximum

puncture resistance is shifted to $\delta_x/L = +0.5$. Finally, a third effect increases F_c in the regions $\delta_y/L = \pm 1$, because tilting of the scale about the x axis not only implies the neighboring scales in the $\delta_y/L = \pm 1$ regions like in the regular array case, but also the scales in the $\delta_x/L = \pm 1$ through the slanted sides of the scales. The overlapped-staggered design has an even high puncture resistance (Fig. 7d). This enhancement is more pronounced along the $\delta_y/L = 0$ line, because tilting of the scale along the y axis involves more neighboring scales. We computed an average puncture resistance of $\bar{F}_c = 8.37$ N for the overlapped design, which is 472% higher than the simple array of scales. Combining Eq. (3) with Eq. (5) gives an average puncture resistance of the staggered design $\bar{F}_c = 11.1$ N, which is 33% higher than the overlapped design and 658% higher than the simple array of scales.

(e) Simplified elasmoid design: In the simplified elasmoid design, we sought to capture the type of multiple overlaps and tilting patterns observed on striped bass (Fig. 1a,b) and other teleost fish. In this design, the base of the scale is shifted along the diagonal ($x = y$) (Fig. 8a). The slant angle employed for this design was the same used for the previous ones, i.e. $\phi = 63.4^\circ$, which led to the same overlapping length, i.e. 4 mm.

The direct effect of this design modification is to resist tilting towards the diagonal direction, so that the region of highest stability is shifted to the point $(\delta_x/L, \delta_y/L) = (0.5, 0.5)$ (Fig. 8b). Here the experimental data points were fitted with the function:

$$F_c = 8.22 \frac{\pi f}{1 - \nu^2} \times \frac{EL^2}{\left(0.08 \left(\frac{\delta_x \cos(\frac{\pi}{4}) + \delta_y \sin(\frac{\pi}{4}) - \delta_{x0}}{L}\right)^2 + \left(\frac{-\delta_x \sin(\frac{\pi}{4}) + \delta_y \cos(\frac{\pi}{4}) - \delta_{y0}}{L}\right)^2\right)^{0.3}} \quad (6)$$

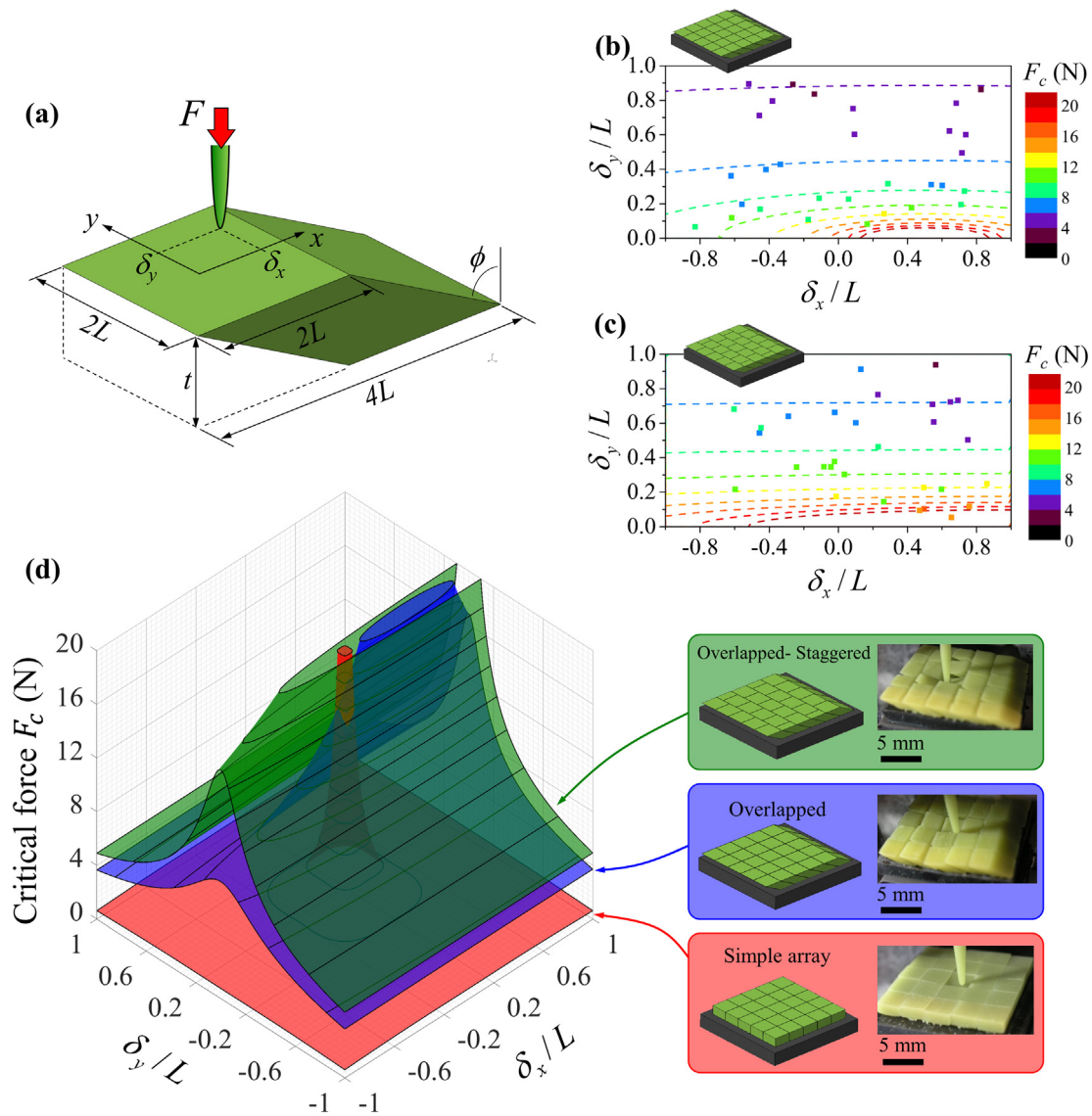


Fig. 7. (a) Diagram of a slanted square used to generate overlapping, with puncture location at offset coordinates (δ_x, δ_y) . Experimental critical puncture force F_c as function of location for (b) the overlapped design and (c) the overlap-staggered design; (d) Surfaces fits of the experimental data with corresponding designs and failure modes. The 2-norm of the fitting errors for the overlapped design and the overlap-staggered design are 4.80 and 9.13, respectively

Fig. 8c shows that the region of high stability is also larger than in the overlapped-staggered design. Near the three corners $(\delta_x/L, \delta_y/L) = (1, -1)$, $(-1, 1)$ and $(-1, -1)$, the two design produce about the same resistance to puncture. The average puncture resistance was $\bar{F}_c = 12.75$ N for the simplified elasmoid design, which is 14% higher than the overlapped-staggered design and 792% higher than the simple array of scales.

(f) Topologically interlocked design: Segmented design made of building blocks with interlocking shapes have recently emerged as a powerful strategy to generate deformation and toughness and otherwise brittle materials [30–33].

A promising design consists of panels made of full or truncated tetrahedral building blocks held in place by a stiff external frame. The interlocking geometry of the assembly is such that the rotation and translation of each block is constrained along all directions by its four neighboring blocks. Here we explored a design that bridges the concept of hard protective scales with the concepts of topological interlocked materials.

The geometry of the scales was obtained from a truncated tetrahedron, as shown on Fig. 9a with a slant angle of $\phi = 31.7^\circ$. By con-

straining the periodicity of the segmentation to be the same as the other designs, i.e. 4 mm, the length of the half edges was $L_x = 2.62$ mm and $L_y = 1.38$ mm. The blocks were arranged in a topologically interlocked array of scale, which was held together by the underlying substrate. The puncture resistance map for this design (Fig. 9b) resembles that of the simple array, and was largely controlled by the offset distance. The results from the topologically interlocked designs were fitted with the function:

$$F_c = 7.79 \frac{\pi f}{1 - \nu^2} \frac{EL^2}{(2.4(\delta_x/L)^2 + (\delta_y/L)^2)^{0.3}} \quad (7)$$

In the y direction, the stability was improved, because of the longer base section. In the x direction the base section was shorter but the stability was still improved because scale-scale

The puncture resistance for this design (Fig. 9c) resembles that of the simple array, but provided an average puncture resistance of $\bar{F}_c = 6.93$ N, which is 3.85 times higher than the puncture resistance of the array of scales. Interactions were promoted by the slanted sides. The performance of the topologically interlocked design was however lower than the staggered design.

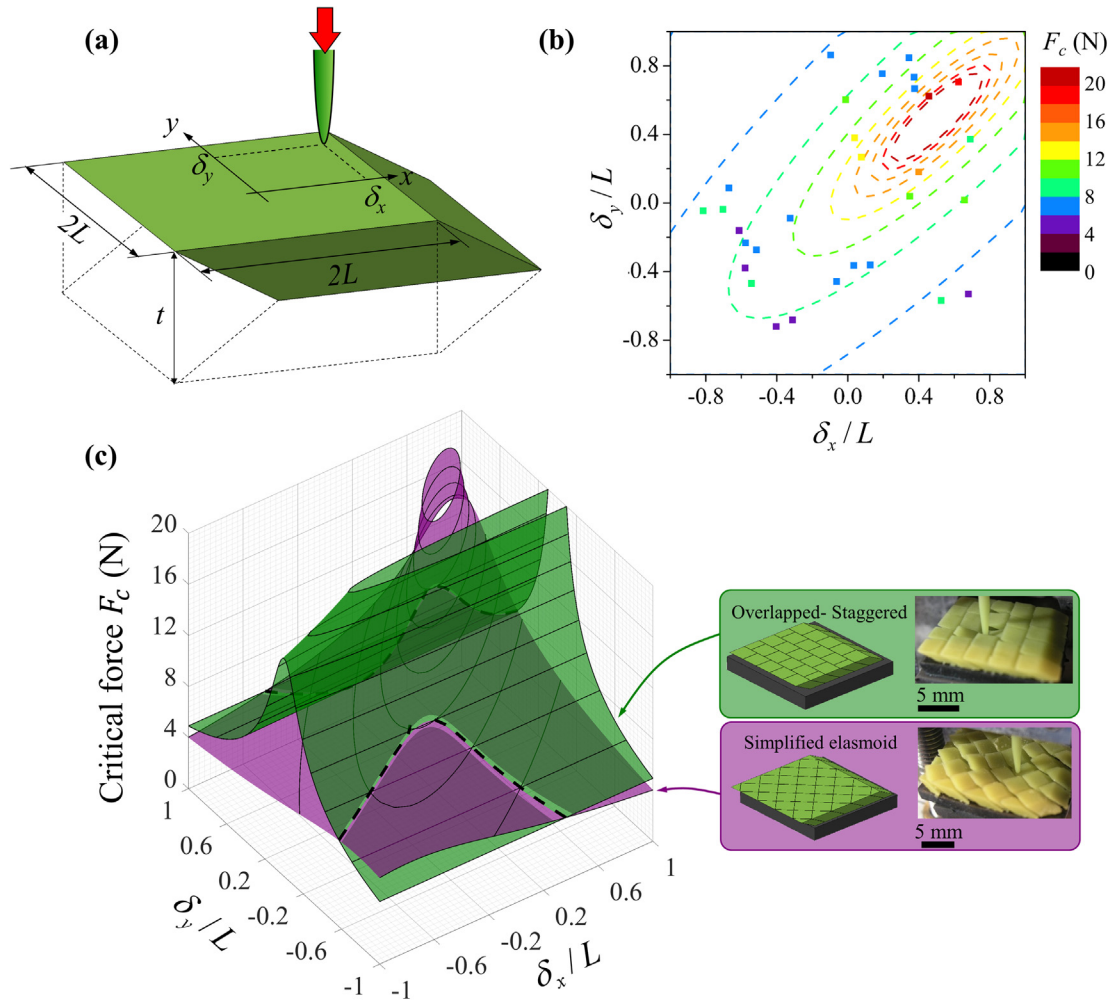


Fig. 8. (a) Diagram of a simplified elasmoid scale. (b) Experimental critical puncture force F_c as function of location; (c) Surfaces fits of the experimental data with corresponding design and failure mode for overlapped-staggered and simplified elasmoid. The 2-norm of the fitting error for the simplified elasmoid design is 12.14.

(g) Simplified ganoid design: Ganoid scales have a complex three-dimensional geometry, which can be broadly described as arrowhead shaped. In addition, the scales of polypterus possess a triangular sharp peg emanating from one of the sides (Fig. 10a). This feature, absent in other ganoid fish such as gar, is believed to imbricate into the neighboring scale to restrict translations and rotations except about the axis of the peg [30]. To test the idea of a stabilizing peg, we started with the overlapped-staggered design, with the addition of a sharp peg of length $d = 2$ mm (Fig. 10a). A cavity of the same geometry and dimension was included on the other side of the scale. The puncture map is shown on Fig. 10b, and this result was fitted with the function:

$$F_c = 11.93 \frac{\pi f}{1 - \nu^2} \times \frac{EL^2}{\left(0.25 \left(\frac{\delta_x \cos(\frac{\pi}{7}) + \delta_y \sin(\frac{\pi}{7}) - \delta_{x0}}{L}\right)^2 + \left(\frac{-\delta_x \sin(\frac{\pi}{7}) + \delta_y \cos(\frac{\pi}{7}) - \delta_{y0}}{L}\right)^2\right)^{0.3}} \quad (8)$$

Fig. 10c shows a comparison of the puncture performance between staggered-overlap and staggered-overlap with side peg (simplified ganoid).

This comparison therefore provides a clear assessment of the effect of the peg: tilting of the scale about the x axis is stabilized, which increases the puncture resistance in the regions $\delta_y/L = \pm 1$.

The puncture resistance is lower in the regions $\delta_x/L = \pm 1$, which may be due to the asymmetry introduced by the peg and socket interlocking. The average puncture resistance for this design is $\bar{F}_c = 12.43$ N, which is 12% higher than what we obtained for the overlapped-staggered design. This result is a good example of how a relatively minor modification to the design of the scales can have profound effects on the stability of the scale.

(h) Full ganoid design: The final design we tested in this study was the full geometry of a polypterus scale obtained from a μ CT scan (Fig. 11). A typical scale from polypterus has a size of about 2.5 mm by 2 mm [19]. All dimensions of the scales were scaled up so that the dimensions of the 3D printed full ganoid scale scales were as close as possible to the previous design (4 mm \times 4 mm). Fig. 11a shows that the puncture resistance is maximum near the protrusion in the $+x, -y$ direction, which suggests that this features has a stabilizing function. In Fig. 11b, the reconstructed puncture resistance surface of the full ganoid design is compared with the puncture resistance surface of the simplified elasmoid design. The function used for fitting the experimental results was:

$$F_c = 7.79 \frac{\pi f}{1 - \nu^2} \times \frac{EL^2}{\left(0.35 \left(\frac{\delta_x \cos(-\frac{\pi}{4}) + \delta_y \sin(-\frac{\pi}{4}) - \delta_{x0}}{L}\right)^2 + \left(\frac{-\delta_x \sin(-\frac{\pi}{4}) + \delta_y \cos(-\frac{\pi}{4}) - \delta_{y0}}{L}\right)^2\right)^{0.4}} \quad (9)$$

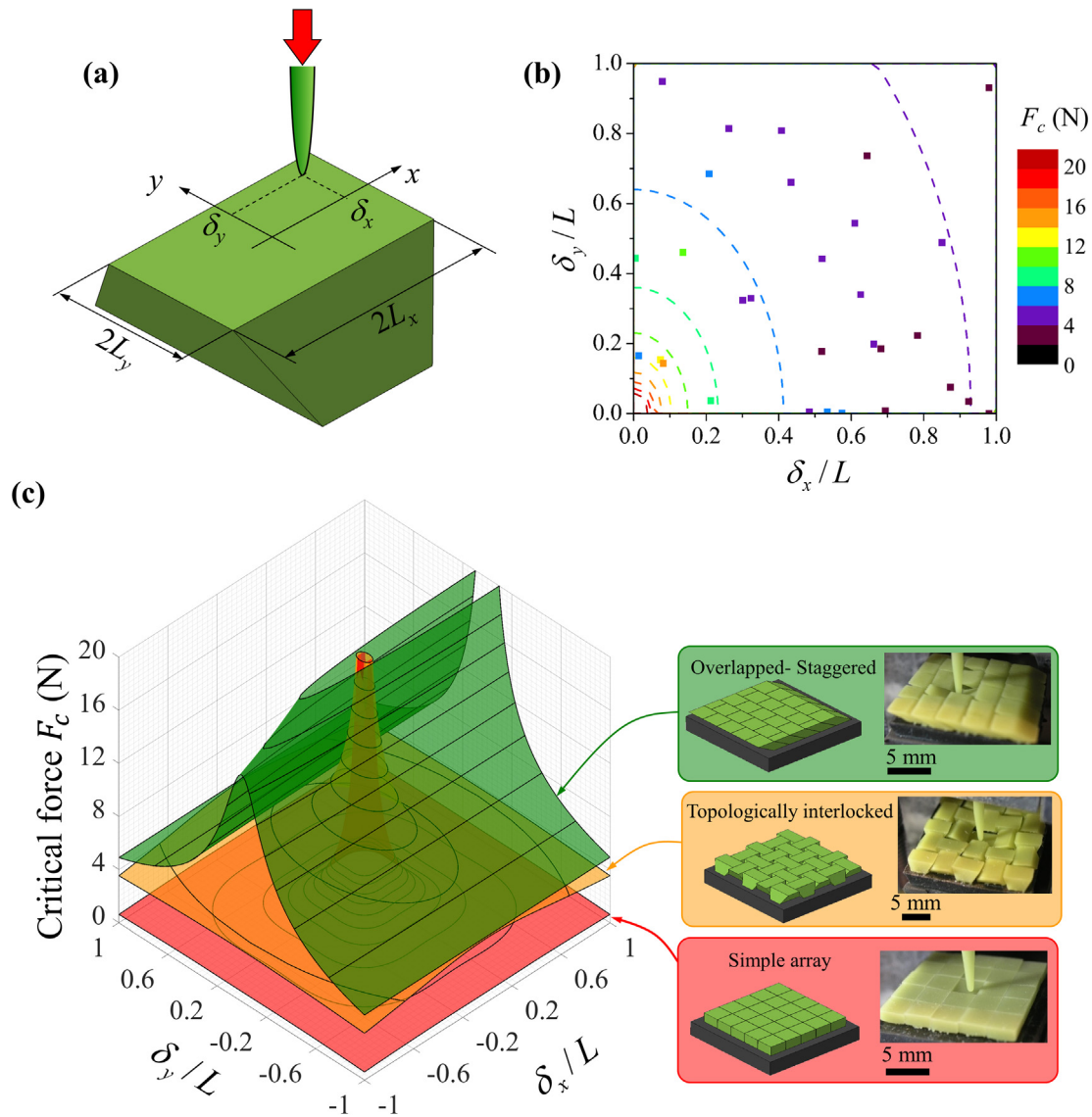


Fig. 9. (a) Diagram of a scale used for the topologically interlocked armor. (b) Critical puncture force F_c as function of location; (c) Surfaces fits of the experimental data with corresponding design and failure mode for overlapped-staggered and topologically interlocked designs. The 2-norm of the fitting error for the topologically interlocked design is 9.53.

The average puncture resistance measured for the polypterus geometry was $\bar{F}_c = 8.56$. Compared to the staggered and the simplified ganoid design, the polypterus scale shows a lower overall puncture resistance, possibly because of the lower degree of overlap of the that polypterus scales ($\eta \sim 25\%$) compared to the other overlapping designs, where $\eta = 50\%$. In the real fish, the presence of stiff collagen fibers connecting neighboring scales may promote the interaction between scales. That polypterus scales, however, performed ~ 5 times better than the simple array of scales.

5. Flexural compliance

For flexible protection, an adequate scaled skin must not only resist puncture, it must also have a high compliance to allow unhindered movements. The same scale-scale interactions that increase puncture resistance may increase the flexural stiffness of the skin. Therefore, each design may be examined as a trade-off between puncture resistance and compliance. To measure the flexural compliance, we used a three-point bending configuration (span = 16 mm) on the same materials used for the puncture tests

(since these tests did not damage the samples). The flexural compliance is defined as the derivative of the force over the deflection, measured at small deflections.

All the tests were performed with the scales on the “intrados” side of the bent samples, so that they increased the stiffness of the sample through their interaction. Bending the scaled skin with the scales on the “extrados side” did not produce any significant stiffening compared to the bare polyurethane membrane because in this configuration the scales move apart from one another [24].

The flexural tests were performed along two perpendicular directions: In the “major overlap” flexural direction, the sample was oriented so that the scales would interact along the direction where the overlap is the highest. The “minor overlap” was the perpendicular direction, which for several design corresponded to a configuration where the scale interacted through sides with smaller or no overlaps. For comparison, we also performed flexural tests on the bare polyurethane membrane. Fig. 12a and b show typical force-deflection curves obtained for all designs and in the major and minor overall configurations. The bare polyurethane membrane produced a linear response with low stiffness, and the

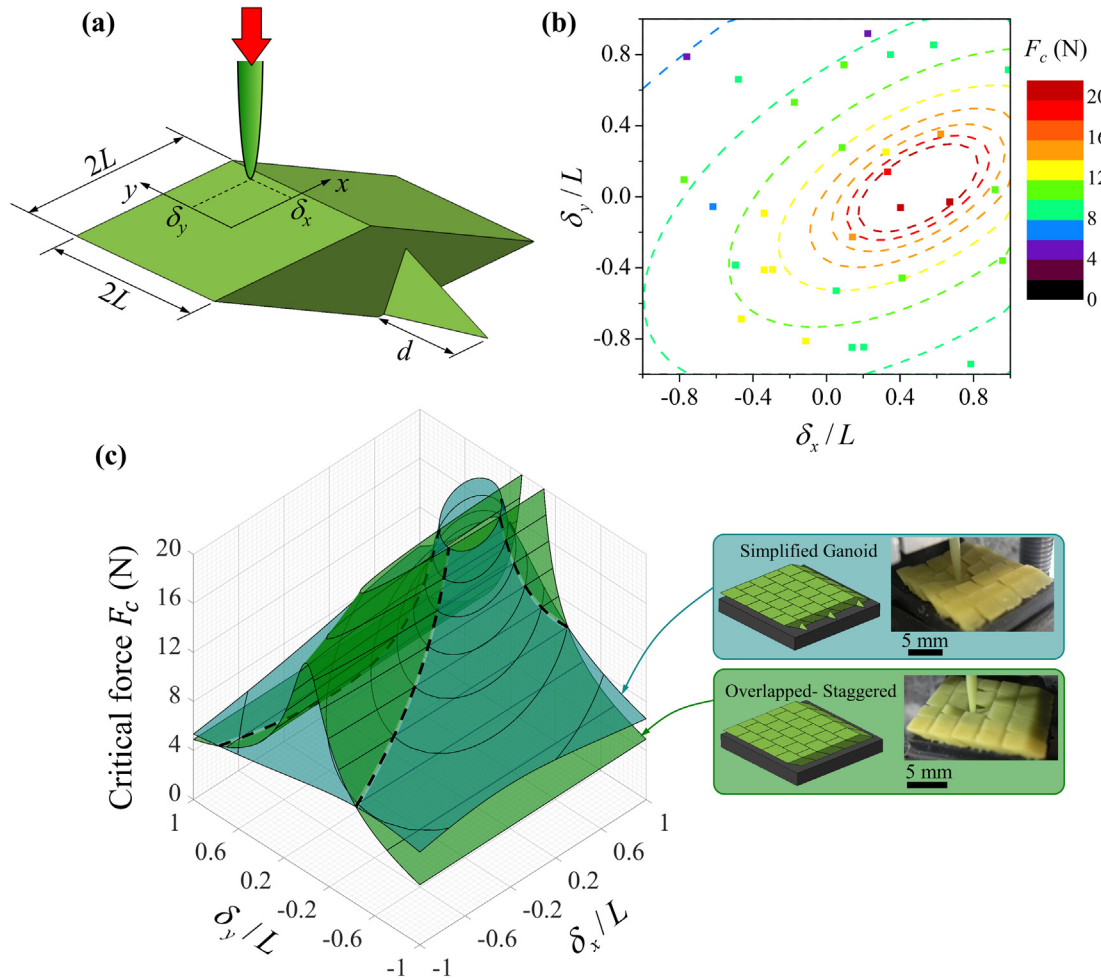


Fig. 10. (a) Diagram of a simplified ganoid scale. (b) Critical puncture force F_c as function of location; (c) Surfaces fits of the experimental data with corresponding design and failure mode for overlapped-staggered and ganoid-like designs. The 2-norm of the fitting error for the topologically interlocked design is 15.32.

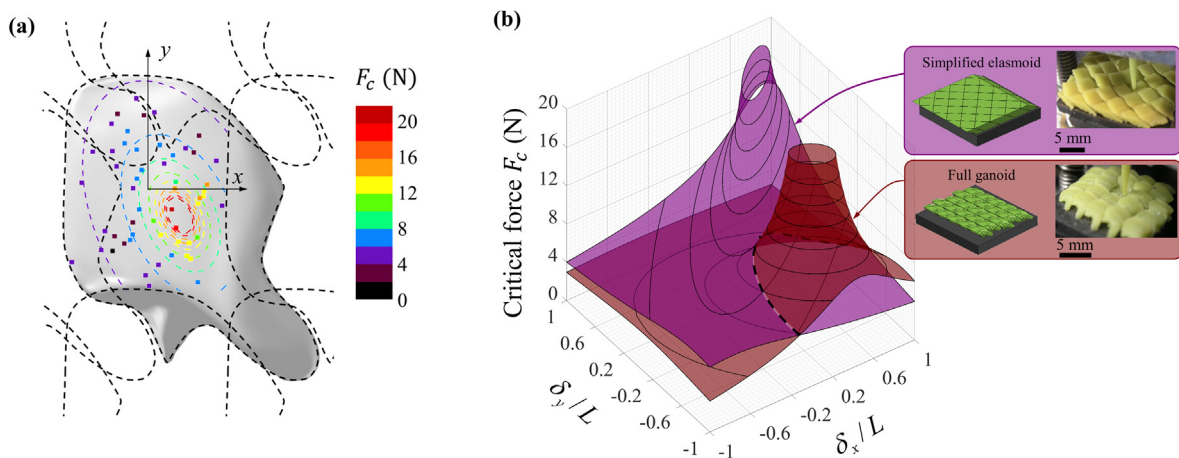


Fig. 11. (a) Diagram of a 3D printed replica of polypterus scale arranged in an array of identical scales, and showing experimental puncture results. (b) Surfaces fits of the experimental data with corresponding design and failure mode for overlapped-staggered and full ganoid designs. The 2-norm of the fitting error for the full ganoid design is 15.92.

isolated scale design produced the same response. For all other designs, scale-scale interactions significantly increased the flexural stiffness, resulting in nonlinear stiffening responses. This observation is in contrast with previous work that reported a linear

response of scaled coating upon bending [17]. In [17] the deflection was accommodated by sharing of the soft matrix between the scales, while in this work, the scaled coating bends by stretching of the membrane, gradual contact of the scales and sliding of the

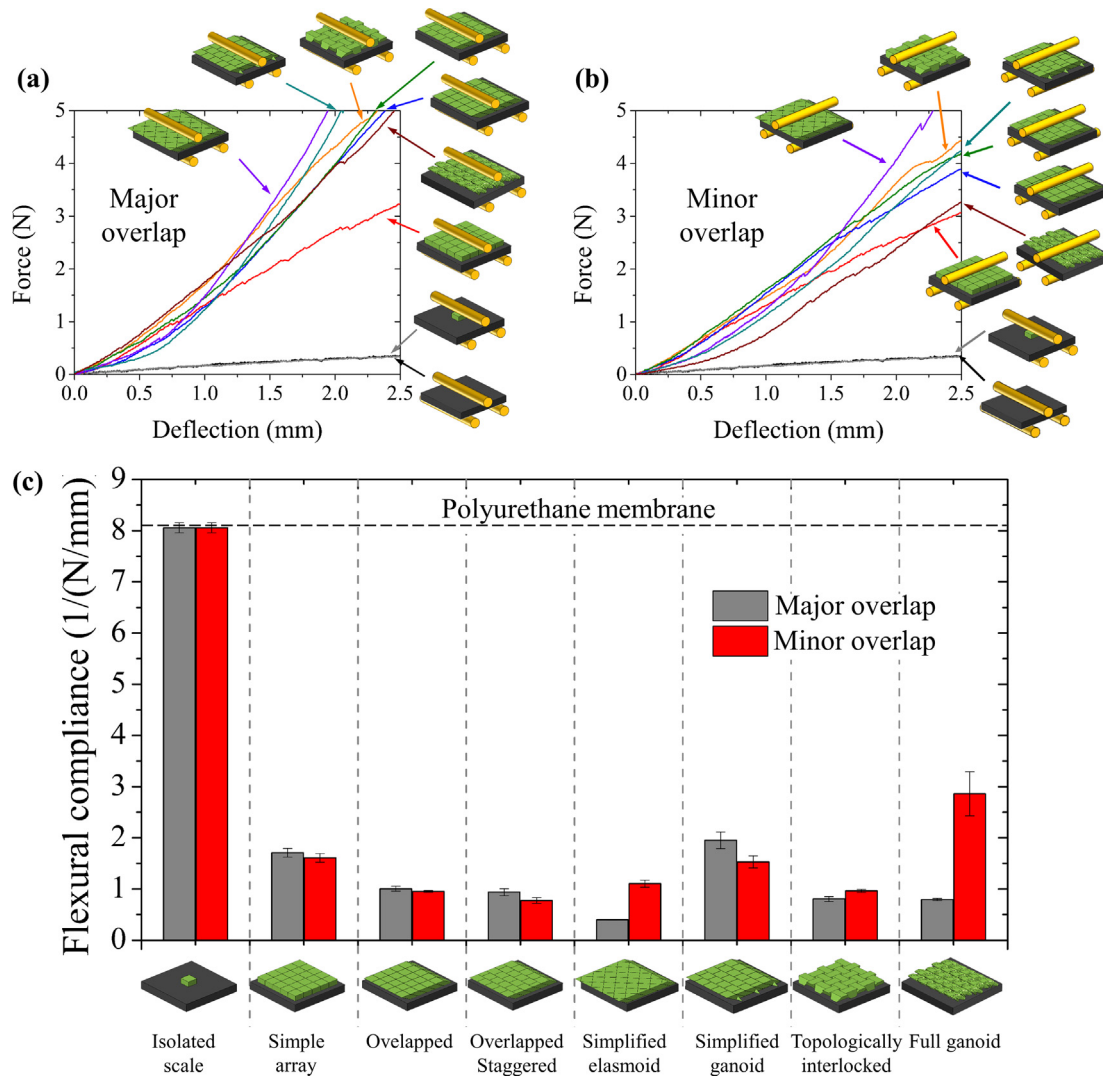


Fig. 12. Force-deflection curves in three-point bending for all the designs and along the directions of (a) major overlap and (b) minor overlap. (c) Comparison of the flexural compliance at small deflections for all the designs considered in this work.

scales. The initial bending compliance was extracted by fitting linearly the force-displacement curves in the deflection range between 0 mm and 0.2 mm, where all the curves behave almost linearly. The flexural compliances at small deflections are compared in Fig. 12c. The bare membrane and isolated scales have by far the highest flexural compliance. The other designs all consist of array of scales, and the interactions between scales decrease the compliance by 60–90%. As expected from the symmetry of the sample, the flexural compliance of the isolated scales and simple array of scales in the major and minor directions are identical. More surprisingly, many of the overlapped design shows similar flexural compliances in the direction of minor and major overlap, regardless of the large difference of overlap in the major overlap direction ($\eta = 50\%$) and minor overlap direction ($\eta = 0\%$). Amongst all the designs analyzed in this work, the elasmoid-like design showed the lowest flexural compliance in the direction of major overlap while, in the direction of minor overlap, the flexural compliance was more compliant than the overlap and staggered designs. Similar observations can be made for the ganoid-like design and the polypterus scales, with the polypterus scales showing the highest compliance amongst all the designs. The data finally shows that the direction of overlap (major/minor) must be taken into account for flexural compliance, and that this factor

must be taken into account in the design of synthetic scaled armors.

6. Summary

To summarize and compare the different designs considered in this work, we display the results in an Ashby chart showing the puncture resistance and flexural compliance (Fig. 13). The chart shows that compared to the isolated scales, the arrays of scales increase the puncture resistance by a factor of 16, but decrease the flexural compliance by a factor of 20. This result indicates that scale-scale interactions significantly increase puncture resistance, but also decrease flexural compliance. Within the designs consisting of array of scales, some geometries and arrangement of scales offered better combination of properties than others, and one of the main result of this work is the large impact of the geometry and arrangement of the scales. As the Ashby chart shows, relatively small changes to the geometry of the scales (with everything else constant) can provide up to tenfold increases in puncture resistance. The worst design for hard-yet-flexible armor is the simple array of scales, which is flexible but provides little resistance upon puncture. Slanting the sides of the scales in overlapping or topolog-

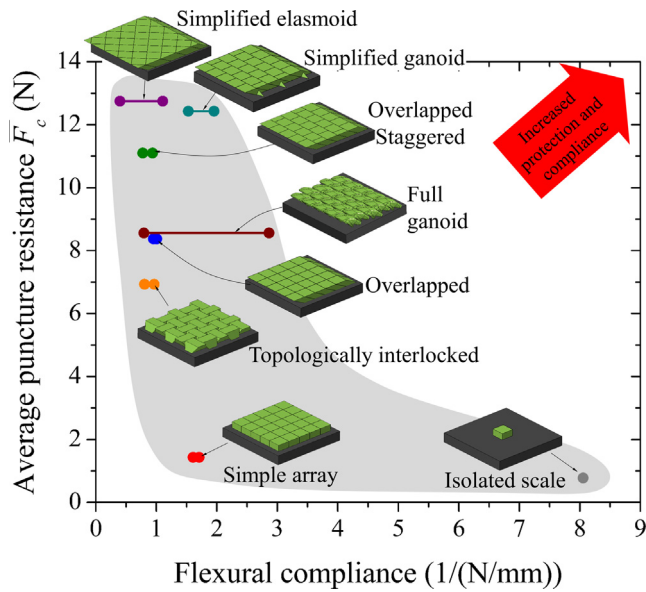


Fig. 13. Ashby chart showing the combinations of flexural compliance and puncture resistance for the different designs considered in this work.

ically interlocked designs increases the resistance to puncture significantly, with only a small loss of flexural compliance. The geometry was enriched further with simplified elasmoid and staggered design, again with little loss in flexural compliance. We found that the elasmoid design produces the scaled skin with the highest puncture resistance, but it was also the design with the lowest flexible compliance. Our results show that more sophisticated features such as side pegs that interlock with neighboring scales provide a promising pathways to increasing the performance of the scales. Compared to the overlapping scaling design, the addition of side pegs not only increased puncture resistance, it also increased flexural compliance. The full polypterus design provided good puncture resistance and high flexural compliance, but exact comparison with the other designs is difficult because the overlap could not be controlled as well. Interestingly, our results show that the simplified ganoid and elasmoid designs, which are close to the geometry and arrangement of natural scales, are among the most efficient designs, providing the highest average puncture resistance and without losing in maximum flexural compliance, as compared to other designs that cover the whole surface. This striking observation suggests that natural evolution has shaped the geometry and arrangement of natural scales to maximize protective efficiency. These findings therefore provide new insights into the mechanisms of natural dermal armor, and also suggest new design strategies for personal protective systems. The indenter material and geometry we have used for these tests were chosen so that the ABS scales behave as hard materials compared to the soft substrate. In actual applications, much harder materials such as high density ceramics should be used for the scales (at least on their front surface) to prevent puncture from sharp objects made of steel or other hard materials. Shape optimization may be coupled with material choice, size and thickness of the scales and attachments of the scales to design and produce high-performance bioinspired flexible armors.

Acknowledgments

This work was supported by a Team Grant from the Fonds de Recherche du Québec – Nature et technologies (FRQNT) and by a

Discovery Grant from the Natural Sciences and Engineering Research Council of Canada. The authors would like to thank Trina Du and Hans Larsson for the microCT data on polypterus scale.

References

- [1] W. Yang, I.H. Chen, B. Gludovatz, E.A. Zimmermann, R.O. Ritchie, M.A. Meyers, Natural flexible dermal armor, *Adv. Mater.* 25 (2013) 31–48.
- [2] W. Yang, V.R. Sherman, B. Gludovatz, E. Schaible, P. Stewart, R.O. Ritchie, M.A. Meyers, On the tear resistance of skin, *Nat. Commun.* 6 (2015) 6649.
- [3] J. Sun, B. Bhushan, Hierarchical structure and mechanical properties of nacre: a review, *RSC Adv.* 2 (20) (2012) 7617.
- [4] M.M. Porter, E. Novitskaya, A.B. Castro-Ceseña, M.A. Meyers, J. McKittrick, Highly deformable bones: unusual deformation mechanisms of seahorse armor, *Acta Biomater.* 9 (6) (2013) 6763–6770.
- [5] R.K. Chintapalli, M. Mirkhalaf, A.K. Dastjerdi, F. Barthelat, Fabrication, testing and modeling of a new flexible armor inspired from natural fish scales and osteoderms, *Bioinspiration Biomimetics* 9 (3) (2014) 36005.
- [6] A.K. Dastjerdi, F. Barthelat, Teleost fish scales amongst the toughest collagenous materials, *J. Mech. Behav. Biomed. Mater.* 52 (2014) 1–13.
- [7] S. Murcia, M. McConville, G. Li, A. Ossa, D. Arola, Temperature effects on the fracture resistance of scales from *Cyprinus carpio*, *Acta Biomater.* 14 (2015) 154–163.
- [8] W. Yang, B. Gludovatz, E.A. Zimmermann, H.A. Bale, R.O. Ritchie, M.A. Meyers, Structure and fracture resistance of alligator gar (*Atractosteus spatula*) armored fish scales, *Acta Biomater.* 9 (4) (2013) 5876–5889.
- [9] P.-Y. Chen, J. Schirer, A. Simpson, R. Nay, Y.-S. Lin, W. Yang, M.I. Lopez, J. Li, E.A. Olevsky, M.A. Meyers, Predation versus protection: fish teeth and scales evaluated by nanoindentation, *J. Mater. Res.* 27 (1) (2012) 100–112.
- [10] M.A. Meyers, Y.S. Lin, E.A. Olevsky, P.Y. Chen, Battle in the Amazon: Arapaima versus piranha, *Adv. Eng. Mater.* 14 (5) (2012) 279–288.
- [11] M.Q. Chandler, P.G. Allison, R.I. Rodriguez, R.D. Moser, A.J. Kennedy, Finite element modeling of multilayered structures of fish scales, *J. Mech. Behav. Biomed. Mater.* 40 (2014) 375–389.
- [12] R. Martini, F. Barthelat, Stability of hard plates on soft substrates and application to the design of bioinspired segmented armor, *J. Mech. Phys. Solids* 92 (2016) 195–209.
- [13] I.H. Chen, J.H. Kiang, V. Correa, M.I. Lopez, P.Y. Chen, J. McKittrick, M.A. Meyers, Armadillo armor: mechanical testing and micro-structural evaluation, *J. Mech. Behav. Biomed. Mater.* 4 (2011) 713–722.
- [14] D. Zhu, L. Szewciw, F. Vernerey, F. Barthelat, Puncture resistance of the scaled skin from striped bass: collective mechanisms and inspiration for new flexible armor designs, *J. Mech. Behav. Biomed. Mater.* 24 (2013) 30–40.
- [15] R. Ghosh, H. Ebrahimi, A. Vaziri, Contact kinematics of biomimetic scales, *Appl. Phys. Lett.* 105 (2014) 2337011–2337014.
- [16] A. Browning, C. Ortiz, M.C. Boyce, Mechanics of composite elasmoid fish scale assemblies and their bioinspired analogues, *J. Mech. Behav. Biomed. Mater.* 19 (2013) 75–86.
- [17] S. Rudykh, C. Ortiz, M.C. Boyce, Flexibility and protection by design: imbricated hybrid microstructures of bio-inspired armor, *Soft Matter* 11 (13) (2015) 2547–2554.
- [18] S. Rudykh, M.C. Boyce, Analysis of elasmoid fish imbricated layered scale-tissue systems and their bio-inspired analogues at finite strains and bending, *IMA J. Appl. Math. (Institute Math. Its Appl)* 79 (5) (2014) 830–847.
- [19] B.J.F. Bruet, J. Song, M.C. Boyce, C. Ortiz, Materials design principles of ancient fish armour, *Nat. Mater.* 7 (9) (2008) 748–756.
- [20] S. Varshney, J. Song, Y. Li, M.C. Boyce, C. Ortiz, Morphometric structural diversity of a natural armor assembly investigated by 2D continuum strain analysis, *J. Struct. Biol.* 192 (3) (2015) 487–499.
- [21] F.J. Vernerey, F. Barthelat, On the mechanics of fishscale structures, *Int. J. Solids Struct.* 47 (17) (2010) 2268–2275.
- [22] F.J. Vernerey, F. Barthelat, Skin and scales of teleost fish: simple structure but high performance and multiple functions, *J. Mech. Phys. Solids* 68 (2014) 66–76.
- [23] V.R. Sherman, H. Quan, W. Yang, R.O. Ritchie, M.A. Meyers, A comparative study of piscine defense: the scales of *Arapaima gigas*, *Latimeria chalumnae* and *Atractosteus spatula*, *J. Mech. Behav. Biomed. Mater.* (2016) 1–16.
- [24] R. Martini, F. Barthelat, Stretch-and-release fabrication, testing and optimization of a flexible ceramic armor inspired from fish scales, *Bioinspiration Biomimetics* 11 (6) (2016) 1–10.
- [25] D. Zhu, C.F. Ortega, R. Motamedi, L. Szewciw, F. Vernerey, F. Barthelat, Structure and mechanical performance of a ‘modern’ fish scale, *Adv. Eng. Mater.* 14 (4) (2012) B185–B194.
- [26] W. Garst, G.S. Garst, Warren and Genevieve Garst Photographic Collection, Colorado State University, 1958.
- [27] P.-Y. Chen, E.E. Novitskaya, M.I. Lopez, C.-Y. Sun, J. McKittrick, Toward a better understanding of mineral microstructure in bony tissues, *Bioinspired Biomimetics Nanobiomater.* 3 (2014) 1–15. July 2016.
- [28] P.J. Blau, The significance and use of the friction coefficient, *Tribol. Int.* 34 (2001) 585–591.
- [29] R. Seidel, K. Lyons, M. Blumer, P. Zaslansky, P. Fratzl, J.C. Weaver, M.N. Dean, Ultrastructural and developmental features of the tessellated endoskeleton of elasmobranchs (sharks and rays), *J. Anat.* (2016).

- [30] J. Duro-Royo, K. Zolotovskiy, L. Mugas-Soldevila, S. Varshney, N. Oxman, M.C. Boyce, C. Ortiz, MetaMesh: a hierarchical computational model for design and fabrication of biomimetic armored surfaces, *CAD Comput. Aided Des.* 60 (2015) 14–27.
- [31] M. Mirkhalaf, J. Tanguay, F. Barthelat, Carving 3D architectures within glass: exploring new strategies to transform the mechanics and performance of materials, *Extreme Mech. Lett.* 7 (2016) 104–113.
- [32] M. Mirkhalaf, A.K. Dastjerdi, F. Barthelat, Overcoming the brittleness of glass through bio-inspiration and micro-architecture, *Nat. Commun.* 5 (2014) 3166.
- [33] L. Djumas, A. Molotnikov, G.P. Simon, Y. Estrin, Enhanced mechanical performance of bio-inspired hybrid structures utilising topological interlocking geometry, *Sci. Rep.* 6 (2016) 26706.